J Mol Model (2013) 19:1445–1450
DOI 10.1007/s00894-012-1702-y

ORIGINAL PAPER

Exohedral and endohedral adsorption of alkaline earth cations in BN nanocluster

Javad Beheshtian · Mohammad Bigdeli Tabar · Zargham Bagheri · Ali Ahmadi Peyghan

Received: 9 July 2012 / Accepted: 19 November 2012 / Published online: 9 December 2012

Abstract Adsorption of three alkaline earth cations inside and outside of a $B_{12}N_{12}$ nano-cage in aqueous medium was investigated using density functional theory. The results obtained are discussed in terms of thermodynamic, geometric, and electronic properties. Based on the calculation of enthalpy changes at 298 K and 1 atm, the adsorption of the considered cations was found to be exothermic outside the cluster while it is endothermic inside. It was also found that the exohedral adsorption favorability of the cluster increases in the series: $Ca^{2+}<Mg^{2+}<<Be^{2+}$ with Gibbs free energy changes in the range of −0.08 to −1.53 eV at B3LYP/6-31G (d) level of theory. Overall, interaction of the cations with the cluster influences the electronic properties of the cluster through stabilizing the HOMO and LUMO as well as reducing the energy gap between them. However, the electronic properties changed much more in the case of endohedral adsorption in comparison with the exohedral adsorption.

Keywords Nanostructure · Fullerene · DFT · Alkaline earth metal

J. Beheshtian
Department of Chemistry, Shahid Rajaee Teacher Training University, PO Box 16875–163, Tehran, Iran

M. B. Tabar · Z. Bagheri
Physics Group, Science Department, Islamic Azad University, Islamshahr Branch, PO Box 33135–369, Islamshahr, Tehran, Iran

A. A. Peyghan (✉)
Young Researchers Club, Islamic Azad University, Islamshahr Branch,
Tehran, Iran
e-mail: ahmadi.iau@gmail.com

Introduction

Since the discovery of C_{60} fullerene, great attention has been focused on synthesis of boron-nitride (BN) fullerene-like nanostructures due to their special electronic, optical, and magnetic properties [1, 2]. For instance, nano-cages may serve as nanocontainers for gas storage, and their BN analogues may also prevent encapsulated particles from oxidization and contamination [3, 4]. Oku et al. [5] synthesized $B_{12}N_{12}$, and showed that these clusters consist of square and hexagonal rings with the band gap energy of 5.1 eV. The structure of the $B_{12}N_{12}$ nano-cage is based on decoration of truncated octahedrons in which all B vertices remain equivalent, as do all N vertices [5]. We have previously shown that $B_{12}N_{12}$ is the most stable nanocluster among the $X_{12}Y_{12}$ (X=Al or B and Y=N or P) cages, being a potential sensor for CO, NO_2, and NO molecules in the presence of H_2, N_2, and CH_4 nanoclusters [6–9].

The main aim of the present research was to study the adsorption of alkaline earth cations inside and outside of the $B_{12}N_{12}$ nano-cage in aqueous medium using density functional theory (DFT), in terms of energetic, structural, and electronic properties. Finding out more about the interactions between these molecules and about the response of the nano-cage towards these ions is necessary to evaluate the potential possibility of fabricating novel $B_{12}N_{12}$-based molecular adsorbent for ion removal or detection in different matrices. In addition, manipulating the properties of nano-cages by cations is an interesting subject in the field of exohedral and endohedral fullerene-based materials. The electronic properties of nano-cages may be altered by the introduction of cations, thereby yielding new materials with tailored properties. In recent years, by increasing the number

of endohedrally substituted atoms, ions, and molecules, proposed applications of fullerene-based materials have been extended, ranging from medicinal (such as drug delivery) to hydrogen storage applications [10, 11].

Despite numerous reports on the endohedral and exohedral carbon fullerenes, there are still a few studies about BN ones [11–13]. For example, La@$B_{36}N_{36}$ endohedral fullerenes have been synthesized by Oku et al. for the first time [12]. They have shown that the $B_{36}N_{36}$ clusters are expanded by introducing doping atoms, resulting in reduced energy gap in the endohedrally La-doped cluster. Elsewhere, spin polarized bonding analysis has been performed on the endohedral alkali-metal-encapsulated $B_{24}N_{24}$ nano-cages (M@$B_{24}N_{24}$, M=Li, Na, K) using DFT with hybrid functional B3LYP to evaluate spin-polarized natural bond orbitals (NBO) [14].

Computational details

Geometry optimizations, density of states (DOS), and natural bond orbital (NBO) analyses have been performed on a $B_{12}N_{12}$, and different X/$B_{12}N_{12}$ complexes (X=Be^{2+}, Mg^{2+}, and Ca^{2+}) at the B3LYP/6-31G(d) level of theory as implemented in GAMESS suite of program [15]. Vibration frequencies have also been calculated at the same level to confirm that all of the stationary points correspond to the true minima on the potential energy surface. The B3LYP density functional has been previously shown to reproduce experimental proprieties [16] and is commonly used for nanostructured materials [17–24]. It has also been demonstrated that the B3LYP provides an efficient and robust basis for calculations of III–V semiconductors by Tomic et al. [25], capable of reliably predicting both the ground state energies and the electronic structure. We have also repeated the calculations at the B3LYP/6-311G (d, p), M06-2X/6-31G (d), and M06-2X/6-311G (d, p) levels of theory. The enthalpy change (ΔH) upon the adsorption of a cation on the $B_{12}N_{12}$ cluster (at T=298 K and P=1 atm) has been defined as follows:

$$\Delta H = H_{complex} - H_{cage} - H_X$$

where $H_{complex}$, H_{cage}, and H_X are the summation of electronic and thermal enthalpies of X/$B_{12}N_{12}$ complex, $B_{12}N_{12}$, and X, respectively, as obtained from the frequency calculations. Basis set superposition error (BSSE) has also been corrected for all interactions using counterpoise method [26–28]. As it is well known, a negative value of ΔH corresponds to an exothermic adsorption. Adsorption energies (ΔE) and Gibbs free energy changes (ΔG) have also been calculated similar to ΔH, using corresponding data at the same conditions. Solvation effects have been included through using the polarizable continuum model (PCM). Dielectric constant of 78.4 has been used for water as the solvent.

Results and discussion

$B_{12}N_{12}$ properties

First, the results will be considered based on the B3LYP/6-31G (d) level of theory. The optimized structure of the pristine $B_{12}N_{12}$ in aqueous medium, and its DOS plot are depicted in Fig. 1, where two types of B–N bonds can be identified: one is shared between two hexagons (α-bond), and the other is shared between a hexagon and a tetragon (β-bond). The bond lengths have been calculated to be about α=1.43 Å and β=1.48 Å. Mulliken population analysis shows a charge transfer of about 0.45 e from the B atom to its neighboring N atoms in the surface of the cluster, which demonstrates the partial ionic nature of the B–N bonds. The DOS plot shows that the $B_{12}N_{12}$ nano-cage is a semi-insulator with a HOMO (highest occupied molecular orbital)/LUMO (the lowest unoccupied molecular orbital) energy gap (E_g) of 6.90 eV. Profiles of HOMO and LUMO of the cluster have been shown in Fig. 1, indicating that they are located mainly on the N and B atoms, respectively. Calculated IR frequencies are found to be in the range of 323.3 to 1,427.5 cm^{-1} in aqueous phase.

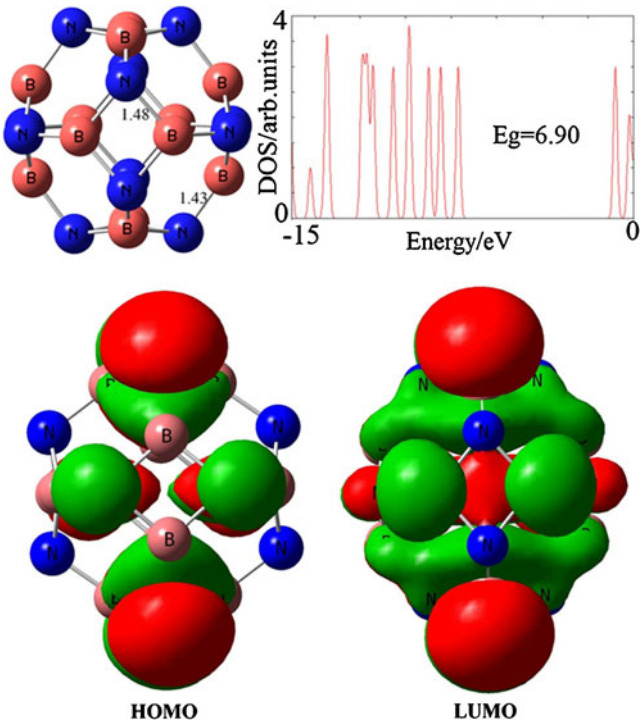

Fig. 1 Optimized structure of $B_{12}N_{12}$ nano-cage, its density of states (DOS) plots, HOMO and LUMO profiles, calculated at B3LYP/6-31G (d) level of theory. Distances are in Ångstroms

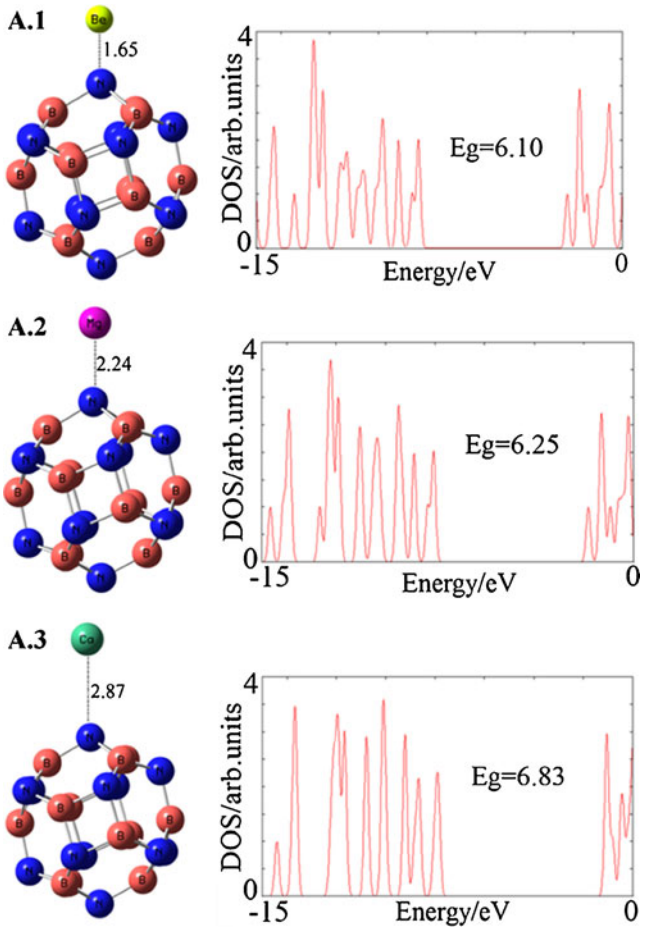

Fig. 2 Optimized structures of exohedral adsorbed alkaline cations on the $B_{12}N_{12}$ and their DOS, calculated at B3LYP/6-31G(d) level of theory. Distances are in Ångstroms

Adsorption of cations on $B_{12}N_{12}$

We first looked for stable configurations (local minima) of the adsorbed alkaline earth cations on the surface of $B_{12}N_{12}$ nano-cage. To this end, the X cation was placed initially at different sites including atop the B or N atom, the bridge site of the α- or β-bond, and above the center of the hexagonal or tetragonal ring. Full structural relaxation, without any constraints, was then performed on each initial configuration. Finally, we obtained only one stable structure with positive vibrational frequencies for every cation in which the cation is located on a N atom of the cluster surface. It should be noted that the X atom in the other initial configurations was reoriented to this site during the fully relaxed optimization. This phenomenon can be rationalized easily by noting the fact that the cations are electron-deficient species that tend to be adsorbed strongly on the electron-rich atoms of nitrogen.

As shown in Fig. 2, the X···N distances increase with increasing atomic number of X (1.65, 2.24, and 2.87 Å for Be^{2+}, Mg^{2+}, and Ca^{2+}, respectively). Also, the corresponding calculated stretching vibrational frequencies of X···N are about 236.2, 101.4, and 65.4 cm^{-1}, respectively. The smaller distance of the Be···N and its much larger stretching vibrational frequency indicate that the interaction of this ion with the cluster should be much stronger than that of the others. This phenomenon is clearly confirmed with the calculated ΔE, ΔH, and ΔG (Table 1). As can be seen from Table 1, the adsorption of cations on the surface of the cluster is exothermic, with negative values for enthalpy changes in all cases. The calculated values for ΔG at 298 K and 1 atm are about −1.50, −0.19, and −0.07 eV, indicating that adsorption of Be^{2+} is thermodynamically much more favorable than that of the other ions. This is may be due to high-density positive charge on the surface of Be^{+} due to its smaller size, which makes it strongly reactive towards electron-rich species. Less negative values of ΔG in comparison with those of ΔH for every cation adsorption indicates that the entropy of the system is decreased upon this process. Our results are comparable with other weak interactions like hydrogen bonding [29–31]. For example, Zhao and Han [30] have shown that the binding energy of the intermolecular hydrogen bond C=O···H=O between the fluorenone chromophore and methanol is about −27.85 kJ/mol^{-1} (−0.29 eV), using DFT method with BP86 functional and TZVP basis set. This value is nearly equal to the adsorption energy of Mg^{2+} on the $B_{12}N_{12}$ and is more and less negative than those of Ca^{2+} and Be^{2+}, respectively.

Table 1 also shows that a quantity of charge is transferred from the cluster to the cation upon the adsorption process.

Table 1 Calculated energetic data, vibrational frequencies (cm^{-1}), HOMO energies (E_{HOMO}), LUMO energies (E_{LUMO}), HOMO-LUMO energy gap (E_g), Fermi level energy (E_{FL}) and the charge on the adsorbate (Q_T, e) for endohedral (**A**) and exohedral (**B**) $B_{12}N_{12}$ nano-cage at B3LYP/6-31G(d) level of theory. Energies are in eV

System	ΔE	ΔH	ΔG	Q_T	υ_{min}	υ_{max}	E_{HOMO}	E_{FL}	E_{LUMO}	E_g	$^{a}\Delta E_g$(%)
$B_{12}N_{12}$	–	–	–	–	329.3	1428.9	−7.70	−4.25	−0.81	6.90	–
A.1 (Be^{+2})	−1.74	−1.70	−1.50	+1.41	239.1	1465.4	−8.36	−5.31	−2.26	6.10	−11.6
A.2 (Mg^{+2})	−0.31	−0.28	−0.19	+1.75	110.7	1449.3	−8.06	−4.94	−1.82	6.25	−9.4
A.3 (Ca^{+2})	−0.10	−0.09	−0.07	+1.90	70.1	1435.2	−7.88	−4.46	−1.05	6.83	−1.0
B.1 (Be^{+2})	4.49	4.57	4.81	−0.33	245.5	1431.2	−9.47	−6.99	−4.51	4.95	−28.2
B.2 (Mg^{+2})	8.98	9.01	9.23	−1.06	331.9	1376.2	−9.41	−6.43	−3.45	5.96	−13.6
B.3 (Ca^{+2})	15.20	15.28	15.95	−0.16	421.0	1298.2	−9.38	−6.54	−3.71	5.67	−17.8

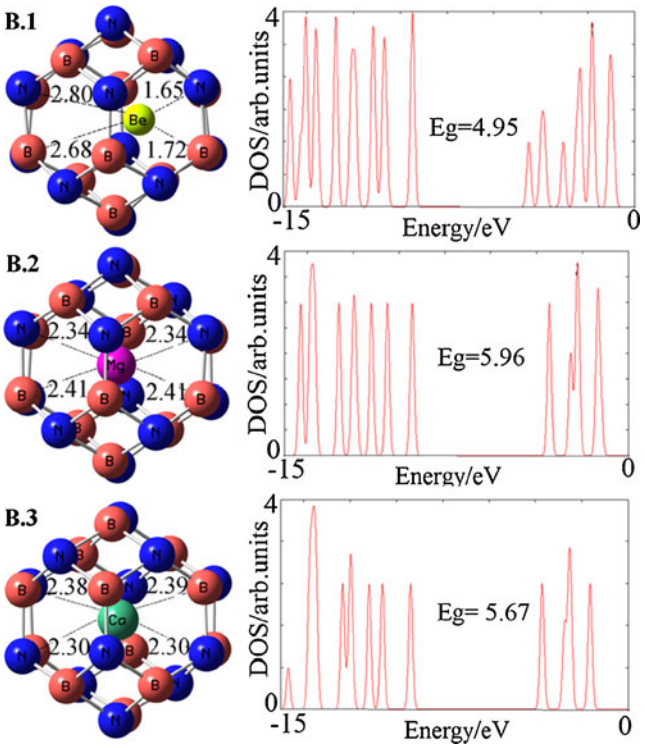

Fig. 3 Optimized structures of endohedral adsorbed alkaline cations on the $B_{12}N_{12}$ and their DOS, calculated at B3LYP/6-31G(d) level of theory. Distances are in Ångstroms

The transferred charge is about 0.59, 0.25, and 0.10 *e* for Be^{2+}, Mg^{2+}, and Ca^{2+}, respectively, indicating that the charge transfer is increased by increasing the strength of the interaction. Also, a local structural deformation around the adsorption sites is predicted. In the $Be^{2+}/B_{12}N_{12}$ complex, the lengths of α and β bonds around the adsorbing N atom are increased significantly to 1.52 and 1.58 Å, respectively. Also, B–N–B angles decreased from 97 ° to 127 ° in the pristine cluster to 76 ° and 105 ° in the Be^{2+}-adsorbed form. NBO analysis demonstrated that hybridization of the adsorbing atom is changed to nearly sp^3. In the Mg^{2+} (Ca^{2+})/$B_{12}N_{12}$ complex, the lengths of α and β bonds increased to 1.48 (1.45) and 1.54 (1.51) Å, respectively, and the B–N–B angles decreased from 97 ° to 127 ° in the pristine cluster to 78.4 ° (79.2 °) and 107.8 ° (108.3 °) in the complex form. The results indicate that structural deformation due to cation adsorption is more considerable in the case of Be^{2+} adsorption, confirming the stronger nature of this process.

Calculated DOS plots in Fig. 2 and data in Table 1 indicate that the HOMO, LUMO, and Fermi level of the cluster are all shifted to lower energies upon adsorption of any of the considered cations. However, the shift of LUMO is considerable in comparison with that of HOMO, which can be attributed to the charge transfer from the cluster to the cations. It is worth mentioning that the canonical assumption for the Fermi level is that in a molecule (at T=0 K), it lies approximately at the middle of E_g. The results also show that the E_g of the cluster is slightly decreased after the adsorption of the cations, especially for the Be^{2+} adsorption. Overall, Be^{2+} has a much greater effect on the electronic properties of the cluster compared to Mg^{2+} and Ca^{2+}.

Endohedral adsorption

The equilibrium structures of ground states for $X@B_{12}N_{12}$ are shown in Fig. 1, and the corresponding electronic structures, calculated energies, and charge transfers are listed in Table 1. We found the average bond lengths of the endohedral cluster to be longer than those of the empty cage, indicating the slight enlargement in sizes of tetragons and hexagons due to encapsulation of the cation. For instance, in $Ca^{2+}@B_{12}N_{12}$, the average length of the α and β bonds is about 1.47 and 1.53, respectively. That is to say, the size of the cage expands along the atomic radii.

As it can be seen from Table 1, in contrast to exohedral adsorption, encapsulation of all cations inside the cluster is endothermic, with positive values for ΔH and ΔG. The calculated ΔG values at 298 K and 1 atm are about 4.85, 9.21, and 15.95 eV for Be^{+2} (**B.1**), Mg^{+2} (**B.2**), and Ca^{+2} (**B.3**), respectively. The results obtained suggest that encapsulation of the cations inside the cluster becomes thermodynamically more unfavorable by increasing the size of the

Table 2 Calculated energetic data, vibrational frequencies (cm^{-1}), HOMO energies (E_{HOMO}), LUMO energies (E_{LUMO}), HOMO–LUMO energy gap (E_g), Fermi level energy (E_{FL}) and the charge on the adsorbate (Q_T, e) for endohedral (**A**) and exohedral (**B**) $B_{12}N_{12}$ nano-cage at B3LYP/6-311G(d, p) level of theory. Energies are in eV

System	ΔE	ΔH	ΔG	Q_T (e)	υ_{min}	υ_{max}	E_{HOMO}	E_{FL}	E_{LUMO}	E_g	$^a\Delta E_g$(%)
$B_{12}N_{12}$	–	–	–	–	327.3	1427.1	−7.96	−4.61	−1.13	6.83	–
A.1 (Be^{+2})	−1.76	−1.65	−1.42	1.557	233.1	1463.1	−8.54	−5.52	−2.50	6.04	−11.6
A.2 (Mg^{+2})	−0.29	−0.25	−0.20	1.098	100.7	1447.4	−8.26	−5.13	−1.99	6.27	−8.2
A.3 (Ca^{+2})	−0.09	−0.08	−0.06	1.766	63.2	1435.5	−8.05	−4.64	−1.23	6.82	−0.1
B.1 (Be^{+2})	4.40	4.42	4.45	−1.63	255.3	1433.1	−9.62	−7.16	−4.69	4.93	−27.8
B.2 (Mg^{+2})	9.02	9.05	9.12	−1.291	337.2	1378.2	−9.63	−6.62	−3.61	6.02	−11.9
B.3 (Ca^{+2})	15.32	15.36	15.40	−1.386	410.2	1299.1	−9.57	−6.74	−3.91	5.66	−17.1

Table 3 Calculated energetic data, vibrational frequencies (cm^{-1}), HOMO energies (E_{HOMO}), LUMO energies (E_{LUMO}), HOMO–LUMO energy gap (E_g), Fermi level energy (E_{FL}) and the charge on the adsorbate (Q_T, e) for endohedral (**A**) and exohedral (**B**) $B_{12}N_{12}$ nano-cage at M06-2X/6-31G(d) level of theory. Energies are in eV

System	ΔE	ΔH	ΔG	Q_T (|e|)	υ_{min}	υ_{max}	E_{HOMO}	E_{FL}	E_{LUMO}	E_g	[a]ΔE_g(%)
$B_{12}N_{12}$	–	–	–	–	333.8	1442.3	−9.27	−4.71	−0.16	9.11	–
A.1 (Be^{+2})	−1.76	−1.71	−1.63	1.158	242.3	1483.5	−9.91	−5.79	−1.67	8.24	−9.5
A.2 (Mg^{+2})	−0.32	−0.26	−0.19	1.440	114.2	1460.3	−9.6	−5.37	−1.14	8.46	−7.5
A.3 (Ca^{+2})	−0.11	−0.10	−0.08	1.750	72.3	1451.4	−9.61	−5.21	−0.82	8.79	−3.9
B.1 (Be^{+2})	4.51	4.53	4.61	−1.416	265.5	1449.7	−11.02	−7.68	−4.34	6.68	−27.0
B.2 (Mg^{+2})	9.10	9.13	9.16	−1.217	342.8	1402.5	−11.53	−7.77	−4.01	7.52	−17.8
B.3 (Ca^{+2})	15.41	15.45	15.50	−1.166	431.8	1315.4	−10.9	−7.355	−3.81	7.09	−22.5

cation. More positive values of ΔG in comparison with those of ΔH indicate that the change of entropy is negative for endohedral adsorption. Interestingly, the calculations show that a large amount of charge is transferred from the cluster to the trapped ions (Table 1), so that the cations are compensated and the system finally becomes partially negative. This may be attributed to the fact that the cations are trapped inside the cluster and have to accept the charge. The quantity of the transferred charge is decreased by increasing the size of the ions.

The calculated DOS plots shown in Fig. 3 and data of Table 1 reveal that, similar to the exohedral adsorption, encapsulation of the alkaline earth cations inside the $B_{12}N_{12}$ nano-cage influences its electronic properties. However, the change in electronic properties in the case of endohedral adsorption is more rigorous than that in the case of exohedral adsorption. The results indicate that the HOMO, Fermi level, and especially the LUMO of the cluster, are shifted appreciably to lower energies so that E_g of the cluster is narrowed. The Be^{+2} encapsulation has more effect on these properties than the other cations. In this case, the LUMO of the cluster becomes sharply more stable by about 4.70 eV, which can be attributed to the large charge transfer from the cluster to the cation. Also the Fermi level decreases significantly from −4.25 eV to −6.99 eV, which leads to an increment in the work function. The work function of a semiconductor is the least amount of the energy required to remove an electron from the Fermi level to a point far enough not to feel any influence from the material. A change in the work function in a semiconductor alters its field emission properties. However, the electron current densities emitted in vacuo are described theoretically by the following classical Richardson-Dushman equation [32, 33]:

$$j = AT^2 \exp(-\Phi/kT)$$

where A is the Richardson constant (A/m^2), T is the temperature (K), and Φ (eV) is the material's work function. After encapsulation of the cations inside the cluster, its work function is increased due to shift of the Fermi level to lower energies. This may arise from a donation of charge from the cluster to the cations. However, as can be seen from Richardson-Dushman equation, the electron current density emitted is related exponentially with negative value of the work function. Therefore, the electron current density emitted from the $B_{12}N_{12}$ cluster will be decreased upon encapsulation of alkaline metal cations.

Finally, we investigated the influence of basis set and functional on the results obtained. To this aim, we repeated the calculations at B3LYP/6-311G (d, p), M06-2X/6-31G

Table 4 Calculated energetic data, vibrational frequencies (cm^{-1}), HOMO energies (E_{HOMO}), LUMO energies (E_{LUMO}), HOMO–LUMO energy gap (E_g), Fermi level energy (E_{FL}) and the charge on the adsorbate (Q_T, e) for endohedral (**A**) and exohedral (**B**) $B_{12}N_{12}$ nano-cage at M06-2X/6-311G (d, p) level of theory. Energies are in eV

System	ΔE	ΔH	ΔG	Q_T (|e|)	υ_{min}	υ_{max}	E_{HOMO}	E_{FL}	E_{LUMO}	E_g	[a]ΔE_g(%)
$B_{12}N_{12}$	–	–	–	–	322.8	1439.2	−9.48	−4.90	−0.33	9.15	–
A.1 (Be^{+2})	−1.78	−1.74	−1.65	1.779	235.6	1479.2	−10.04	−5.98	−1.93	8.11	−11.4
A.2 (Mg^{+2})	−0.34	−0.29	−0.21	1.314	110.8	1457.1	−9.85	−5.71	−1.58	8.27	−9.6
A.3 (Ca^{+2})	−0.15	−0.14	−0.10	1.834	69.2	1448.9	−9.61	−5.31	−1.01	8.60	−6.0
B.1 (Be^{+2})	4.50	4.51	4.59	−1.257	260.7	1445.1	−11.15	−7.82	−4.5	6.65	−27.3
B.2 (Mg^{+2})	9.07	9.11	9.15	−1.788	339.1	1400.1	−11.2	−7.45	−3.71	7.49	−18.1
B.3 (Ca^{+2})	15.32	15.35	15.41	−1.575	425.9	1312.2	−11.22	−7.78	−4.34	6.88	−24.8

(d), and M06-2X/6-311G (d, p) levels of theory, and have summarized the results in Tables 2, 3 and 4. Table 2 shows the results obtained by B3LYP/6-311G (d, p), indicating that using a larger basis set in comparison with the 6–31G (d) slightly influences the results. Like the results obtained through 6–31G (d), the endohedral and exohedral adsorptions are endothermic and exothermic at 6–311G (d, p) level, respectively. The values of ΔE, ΔH, and ΔG obtained with the larger basis set show negligible deviation from the results calculated by 6–31G (d). Also, it was found that the vibrational frequencies and electronic properties did not change significantly using the larger basis set. Tables 3 and 4 show the results of M06-2X functional with 6–31G (d) and 6–311G (d, p) basis sets, respectively. It can be seen that their ΔE, ΔH, and ΔG results are in good agreement with those obtained by B3LYP, while the calculated electronic properties of the HOMO, LUMO, Fermi level, and E_g depend on the kind of functional used. For example, the M06-2X values of E_g are larger than those of the B3LYP. It can be concluded that the results may experience more change through using different functionals, compared to utilizing various basis sets.

Conclusions

We studied exohedral and endohedral adsorption of alkaline earth cations inside and outside of $B_{12}N_{12}$ nanocage in aqueous medium using DFT in terms of thermodynamic, geometric, and electronic properties. The adsorption of cations was found to be exothermic outside but endothermic inside the cluster. The adsorption favorability increased in the series: $Ca^{2+}<Mg^{2+}<<Be^{2+}$. The electronic properties of the cluster changed much more in the case of endohedral adsorption in comparison with the exohedral adsorption due to significant charge transfer from the cluster to the cations in the former. Moreover, endohedral adsorption significantly increases the work function of the cluster, impeding the field electron emission from the cluster surface based on the Richardson-Dushman equation.

References

1. Koi N, Oku T, Narita I, Suganuma K (2005) Diamond Relat Mater 14:1190–1192
2. Pan Y, Huo K, Hu Y et al (2005) Small 1:1199–1203
3. Terrones M, Kamalakaran R, Seeger T, Rühle M (2000) Chem-Comm 23:2335–2336
4. Kitahara H, Oku T, Hirano T, Suganuma K (2001) Diamond Relat Mater 10:1210–1213
5. Oku T, Nishiwaki A, Narita I (2004) Sci Technol Adv Mater 5:635–638
6. Beheshtian J, Bagheri Z, Kamfiroozi M, Ahmadi A (2011) Microelectron J 42:1400–1403
7. Beheshtian J, Ahmadi A, Bagheri Z, Kamfiroozi M (2011) Struct Chem 22:183–188
8. Beheshtian J, Kamfiroozi M, Bagheri Z, Ahmadi A (2012) Chin J Chem Phys 25:60–64
9. Beheshtian J, Bagheri Z, Kamfiroozi M, Ahmadi A (2012) J Mol Model 18:2653–2658
10. Cagle D, Kennel S, Saed M, Alford J, Wilson L (1999) Proc Natl Acad Sci USA 96:5182–5187
11. Komatsu K, Murata M, Murata Y (2005) Science 307:238–240
12. Oku T, Kuno M, Narita I (2002) Diamond Relat Mater 11:940–944
13. Kuno M, Oku T, Suganuma K (2001) Scr Mater 44:1583–1586
14. Oliaey AR, Boshra A, Khavary M (2010) Physica E 42:2314–2318
15. Schmidt M et al (1993) J Comput Chem 14:1347–1363
16. Bauschlicher CW (1995) Chem Phys Lett 246:40–44
17. Ahmadi A, Hadipour NL, Kamfiroozi M, Bagheri Z (2012) Sens Actuators B-Chem 161:1025–1029
18. Dinadayalane TC, Murray JS, Concha MC, Politzer P, Leszczynski J (2010) J Chem Theor Comp 6:1351–1357
19. Beheshtian J, Baei MT, Ahmadi A (2012) Surf Sci 606:981–985
20. Wu H-S, Cui X-Y, Qin X-F, Strout D, Jiao H (2006) J Mol Model 12:537–542
21. Beheshtian J, Peyghan A, Bagheri Z, Kamfiroozi M (2012) Struct Chem 23:1567–1572
22. Beheshtian J, Baei M, Peyghan A, Bagheri Z (2012) J Mol Model 18:4745–4750
23. Beheshtian J, Soleymanabadi H, Kamfiroozi M, Ahmadi A (2012) J Mol Model 18:2343–2348
24. Ahmadi A, Beheshtian J, Kamfiroozi M (2012) J Mol Model 18:1729–1734
25. Tomić S, Montanari B, Harrison NM (2008) Phys E 40:2125–2127
26. Salvador P, Paizs B, Duran M, Suhai S (2001) J Comput Chem 22:765–786
27. Boys SF, Bernardi F (1970) Mol Phys 19:553–566
28. Jansen HB, Ros P (1969) Chem Phys Lett 3(3):140–143
29. Zhao G-J, Han K-L (2008) Biophys J 94:38–46
30. Zhao G-J, Han K-L (2012) Acc Chem Res 45:404–413
31. Zhao G-J, Liu J-Y, Zhou L-C, Han K-L (2007) J Phys Chem B 111:8940–8945
32. Richardson OW (1924) Phys Rev 23:153–155
33. Dushman S (1930) Rev Mod Phys 2:381–476